JACS
JOURNAL OF THE AMERICAN CHEMICAL SOCIETY

pubs.acs.org/JACS

Article

Amino Acid Residues Determine the Response of Flexible Metal–Organic Frameworks to Guests

Yong Yan, Elliot J. Carrington, Rémi Pétuya, George F. S. Whitehead, Ajay Verma, Rebecca K. Hylton, Chiu C. Tang, Neil G. Berry, George R. Darling, Matthew S. Dyer, Dmytro Antypov, Alexandros P. Katsoulidis, and Matthew J. Rosseinsky*

Cite This: J. Am. Chem. Soc. 2020, 142, 14903–14913

Read Online

ACCESS | Metrics & More | Article Recommendations | Supporting Information

ABSTRACT: Flexible metal–organic frameworks (MOFs) undergo structural transformations in response to physical and chemical stimuli. This is hard to control because of feedback between guest uptake and host structure change. We report a family of flexible MOFs based on derivatized amino acid linkers. Their porosity consists of a one-dimensional channel connected to three peripheral pockets. This network structure amplifies small local changes in linker conformation, which are strongly coupled to the guest packing in and the shape of the peripheral pockets, to afford large changes in the global pore geometry that can, for example, segment the pore into four isolated components. The synergy among pore volume, guest packing, and linker conformation that characterizes this family of structures can be determined by the amino acid side chain, because it is repositioned by linker torsion. The resulting control optimizes noncovalent interactions to differentiate the uptake and structure response of host–guest pairs with similar chemistries.

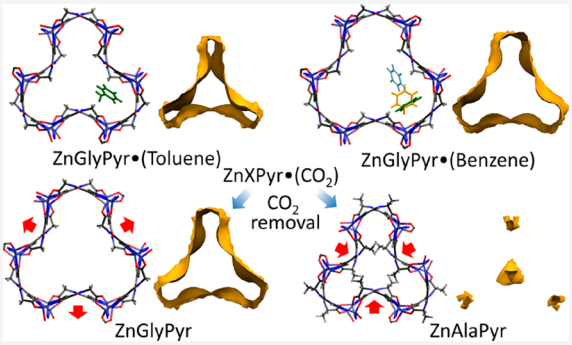

INTRODUCTION

Flexible metal–organic frameworks (MOFs) are a class of crystalline porous materials formed by coordination bonds between organic linkers and metal ions or clusters where the framework structure changes upon external stimuli. Flexible MOFs can adapt their pore shape and chemistry to suit process requirements in separation,[1−3] sensing,[4,5] storage,[6,7] and catalysis applications.[8] These structural changes occur through a variety of mechanisms, including the conformational change of an organic linker,[9−11] a modification of the coordination environment of the metal ions in the secondary building unit (SBU),[12,13] the hinge motion of coordinated carboxylate groups,[14−17] or the movement of interpenetrated networks relative to each other.[18,19] In contrast with rigid porous materials, porous hosts such as flexible frameworks,[20] interpenetrated cages,[21] and synthetic receptors[22] can change their pore volume and shape when they interact with guests, producing a feedback between guest uptake and host structure that is difficult to control. Control of guest uptake by rigid materials through chemical modification, for example, addition of functional groups to the linkers in rigid MOFs, is well understood in terms of the resulting fixed changes to pore shape[23] and guest interactions[24,25] and offers an opportunity to direct the response of flexible systems.[26] The complex feedback in the flexible case requires consideration of the host–guest system in understanding the observed structural and chemical response.

One effective method for synthesizing flexible porous materials employs peptide-based linkers that can adopt several conformations through the changes in torsion angles around their sp^3 carbon (Cα of the amino acids forming the peptide).[27−31] These porous hosts have conformational energy landscapes with certain analogies to those of protein structures and perform chemical functions in response to changes in their pore content.[31] However, the structural and compositional diversity of these families of MOFs remains limited if only naturally occurring peptide molecules are used as linkers. The coordination chemistry of the terminal carboxylate and amino groups prevents the formation of many well-known SBUs and restricts the number and nature of accessible topologies.

To expand the linker–metal coordination chemistry while retaining conformational and side chain diversity, we have developed a family of linkers (XPyr) where an amino acid (X) is coupled with a pyrazole (Pyr) compound through an amide

Received: April 8, 2020
Published: July 25, 2020

https://dx.doi.org/10.1021/jacs.0c03853
J. Am. Chem. Soc. 2020, 142, 14903−14913

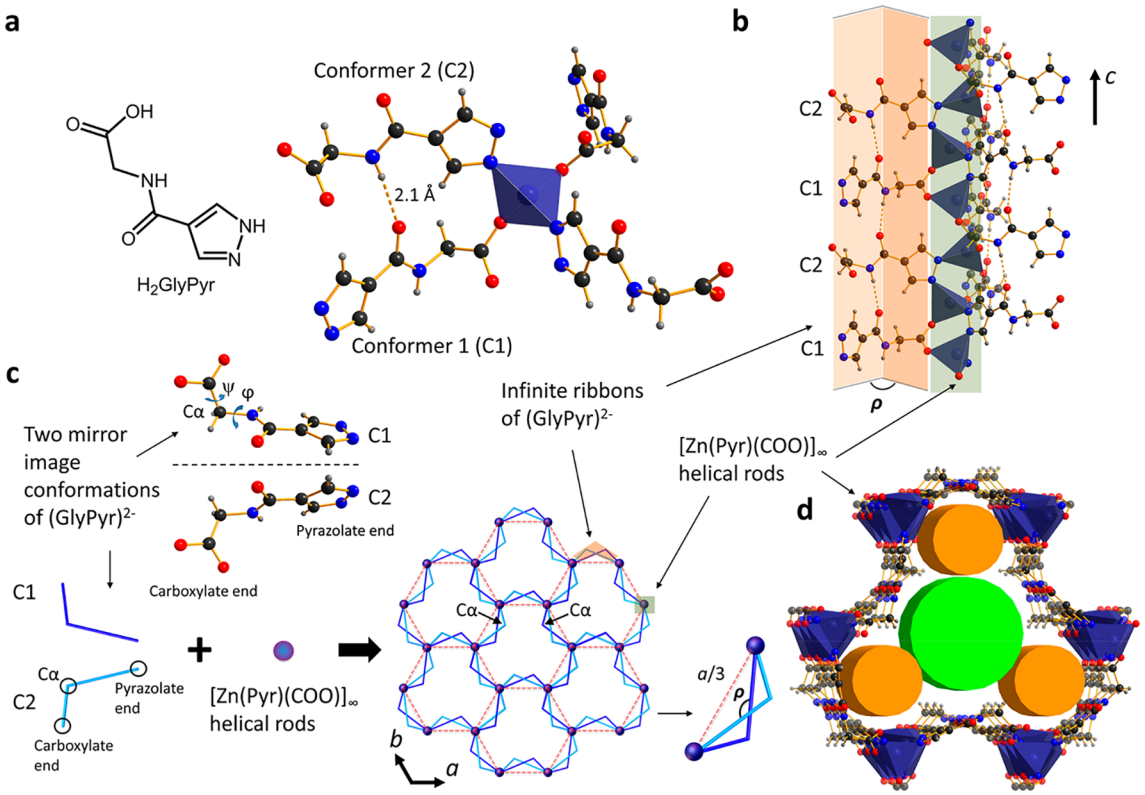

Figure 1. Linker conformation determining the nonuniform pore topology of ZnGlyPyr•(DMF). (a) The linker H_2GlyPyr and the tetrahedral ZnO_2N_2 coordination environment of the Zn(II) ions in the ZnGlyPyr framework. (b) The $[Zn(Pyr)(COO)]_\infty$ helical rods (shaded light green) connected to the bent ribbons (shaded orange) of kinked H-bonded $(GlyPyr)^{2-}$ linkers both running along the *c* axis. (c) Two kinked mirror-image conformers, C1 and C2 of $(GlyPyr)^{2-}$ (φ = 87.3° and ψ = −145.6° for C1 and φ = −87.3° and ψ = 145.6° for C2), arranged in an antiparallel alternating manner along the *c* axis, forming infinite H-bonded ribbons, which connect each $[Zn(Pyr)(COO)]_\infty$ chain to three other chains to form a honeycomb net. The bend in the ribbons is defined by the angle ρ arising from the linker conformation. (d) The channel running along the *c* axis of ZnGlyPyr•(DMF) molecules in the pore are omitted for clarity. The accessible void can be divided into a central channel (green) and three peripheral pockets (orange). Atom colors: C, black; H, gray; O, red; N, blue; Zn, indigo.

bond, forming molecules which terminate in both carboxylic and pyrazole groups that each have extensive framework-forming chemistry.[32−35] This preserves the conformational space associated with oligopeptides, through the presence of the sp^3 carbon, while the coordination modes of the terminal groups facilitate the formation of a variety of SBUs. Chemical diversity is also maintained, as linkers based on all amino acid residues are potentially accessible. In biological systems, this diversity in functionalization of amino acids determines the response of protein structures to their chemical environment through torsional control of side chain position and extended backbone structure.[36,37] A specific example is the substitution of glycine (Gly) with alanine (Ala) in α-helices, which stabilizes a folded structure over a fully flexible denatured state[38−40] because Gly has higher conformational entropy than Ala, while Ala increases the side chain−side chain interactions that favor folded states.[41,42] The peptide-derived XPyr linkers afford new isoreticular flexible MOFs, with the formula ZnXPyr, on the basis of coordination chemistry distinct from that available to peptides, and contain large one-dimensional pores with a complex geometry where narrow pockets and wider channels coexist. Linker conformational change both reconfigures the global pore shape and locally relocates the amino acid derived side chain to recognize chemically similar guests. The structural response of each framework to guests is distinct, coupling their organization in the pockets to the resulting pore volume and the overall number of guests taken up.

RESULTS AND DISCUSSION

Structure of ZnGlyPyr•(DMF). H_2GlyPyr (Figure 1a), synthesized via an amide coupling reaction involving a protected glycine moiety (see section S2 in the Supporting Information, Figures S1−S9), was reacted solvothermally with $Zn(NO_3)_2{\cdot}6H_2O$ in *N,N*-dimethylformamide (DMF) to give ZnGlyPyr•(DMF): containing 1.2 DMF per formula unit (see section S3 in the Supporting Information). Single crystal X-ray diffraction (SCXRD) data collected at 100 K showed that ZnGlyPyr•(DMF) crystallizes in trigonal space group *R*3*c*, with unit cell dimensions *a* = 28.7263 Å, *c* = 10.1348 Å, *V* = 7242.8 $Å^3$. Removing the modeled DMF guests and calculating the accessible pore volume gives a value of 4411 $Å^3$ (60.9%). The bulk phase purity of ZnGlyPyr•(DMF) was confirmed by powder X-ray diffraction (PXRD) (Figure S12). ZnGlyPyr•(DMF) is not soluble in common organic solvents such as MeOH, benzene, and toluene (Figures S13−S15).

The pyrazole and carboxylic acid groups of the linker are both deprotonated and coordinate to Zn(II) ions in tetrahedral ZnO_2N_2 units (Figure 1a). These tetrahedra are connected via both the pyrazolate and carboxylate groups in μ_2 bridging modes to form infinite $[Zn(Pyr)(COO)]_\infty$ helical rods, half left handed and half right handed, which run along the crystallographic *c* axis (Figure 1b). Each helical [Zn(Pyr)-

https://dx.doi.org/10.1021/jacs.0c03853
J. Am. Chem. Soc. 2020, 142, 14903−14913

$(COO)]_\infty$ rod is connected to three opposite handed rods via infinite ribbons of NH···OC H-bonded linkers, generating a honeycomb net (Figure 1c). The framework topology is *etb*[43,44] with a one-dimensional pore running parallel to the *c* axis defined by six rods and six ribbons. The $(GlyPyr)^{2-}$ linker adopts two nonsuperimposable kinked mirror-image conformations (conformers 1 and 2, denoted C1 and C2, respectively, in Figure 1). These conformers are accessed by opposite rotations about the N−Cα and Cα−C bonds of the Gly unit (torsion angles φ and ψ in Figure 1c) by 92.7° and 34.4°, respectively, from their equilibrium values of 180° in the lowest energy conformation of the free linker, at a torsional energy cost of 10.8 kJ/mol (Figure S17). The two $(GlyPyr)^{2-}$ conformers are arranged antiparallel to each other along the pore direction (Figure 1b and Figure S18). This arrangement of kinked mirror-image linkers imposes a bent configuration on the infinite ribbons which protrude alternately in and out of a regular hexagon (Figure 1c). The trefoil-shaped pore imposed by the linker conformation can be considered as a central channel, which could hold an 8.2 Å diameter cylinder, connected to three adjoining peripheral pockets, which could each fit a 5.4 Å cylinder (Figure 1d). The deviation of the pore shape from the regular hexagon is quantified by the angle ρ of the bent ribbons, which is determined by the linker conformation (ρ is defined in section S4 in the Supporting Information and Figures S19 and S20). The as-synthesized ZnGlyPyr•(DMF) has a ρ value of 132.2°, a significant distortion from the 180° angle of a hexagonal pore constructed from straight linkers in the free linker equilibrium conformation.

Isoreticular ZnAlaPyr•(DMF). The narrowest part of the trefoil-shaped pore of the ZnGlyPyr framework, referred to hereafter as the pinch point, is located at the entrance connecting the peripheral pocket to the central channel, where the glycine Cα resides (Figure 1c). As amino acid substituents will occupy this pinch point position, they can be expected to control the structural and uptake response to guests if an isoreticular series can be prepared. The contrasting structure-determining roles of Gly and Ala in α-helix-based proteins and the role of linker conformation in determining both the pore shape and the side chain location in ZnGlyPyr motivated the synthesis of ZnAlaPyr. L-H_2AlaPyr (Figure 2a) was prepared through replacement of glycine with L-alanine in the linker synthesis and was reacted with $Zn(NO_3)_2{\cdot}6H_2O$ and a small amount of hydrochloric acid in DMF to produce ZnAlaPyr (see sections S5 and S6 in the Supporting Information, Figures S21−S30). The linker retained its chirality after MOF formation, and ZnAlaPyr crystallized in the lower symmetry space group *R*3. The $(L\text{-}AlaPyr)^{2-}$ linker adopts two conformations which are no longer symmetry-related, unlike the Gly analogue, and are both present in the asymmetric unit (Figure 2b,c). The as-made material ZnAlaPyr•(DMF) is isoreticular to ZnGlyPyr•(DMF), with a unit cell volume of 7308 $Å^3$ and a ρ value of 135.4°. The ZnXPyr framework directs the Ala side chains into the channel space, reducing the overall void volume (56.4% in ZnAlaPyr in comparison to 61.2% in ZnGlyPyr) (Figure 2d and Figure S31). The opposing methyl groups on either side of the pinch point now significantly reduce the shortest wall-to-wall distance across the pore from 5.5 to 3.1 Å (Figure 2d and Figure S32; all interatomic distances are quoted with the van der Waals (vdW) radii of the atoms subtracted).

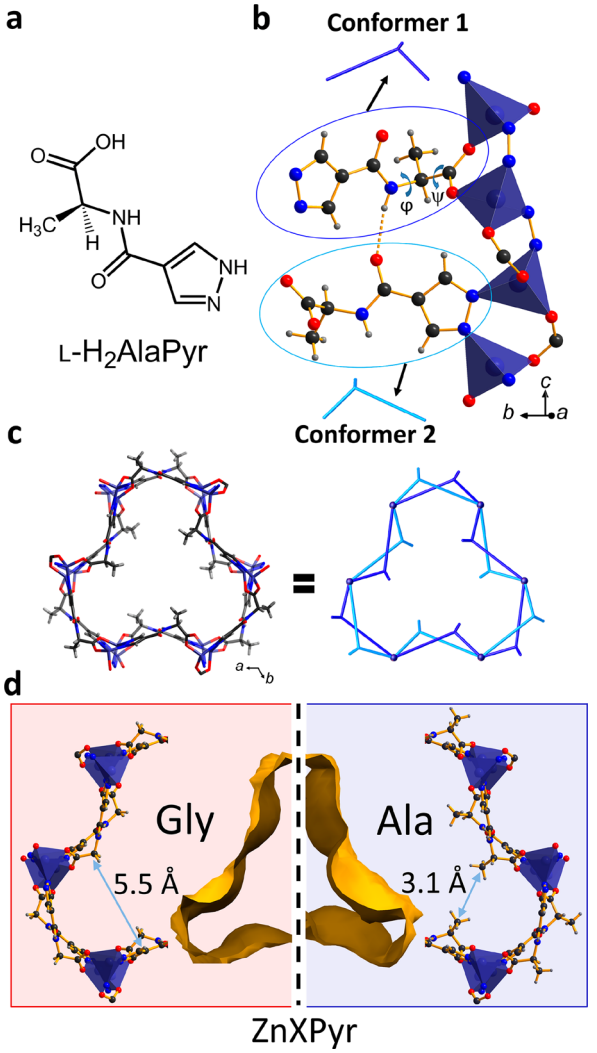

Figure 2. Side chain variation in ZnGlyPyr resulting in the synthesis of isoreticular ZnAlaPyr•(DMF). (a) Structure of L-H_2AlaPyr. (b) SCXRD structure of ZnAlaPyr•(DMF) showing the two linker conformers of $(L\text{-}AlaPyr)^{2-}$ (colored as blue and light blue schematics, respectively) arranged in an antiparallel fashion along the *c* axis. These two $(L\text{-}AlaPyr)^{2-}$ conformers are not symmetry-related (φ = 71.8° and ψ = −139.5° for conformer 1; φ = −91.1° and ψ = 138.2° for conformer 2). (c) View of the pore structure of ZnAlaPyr•(DMF) on the *ab* plane and its schematic representation with the two types of linker conformers. (d) Schematic constructed from the left-hand side of one pore of ZnGlyPyr (shaded red) and the right-hand side of one pore of ZnAlaPyr (shaded blue), illustrating the narrowing of the pinch point between the central channel and pockets produced by the Ala methyl side chain. The C···C distance is measured between the two closest C atoms across the pinch point (with the vdW radii of the atoms taken into account) for each structure. The solvent-accessible surface with probe radius 1.2 Å illustrates the resulted change in pore size and shape by the methyl side chain. Atom colors: Zn, indigo; C, gray; H, light gray; N, blue; O, red. DMF molecules in the structures are omitted for clarity.

Structural Flexibility of ZnGlyPyr and ZnAlaPyr. The structural response of both frameworks was explored by exchanging the DMF molecules in the pores of the as-made materials with a library of 17 different liquid guests (see section S7 in the Supporting Information), giving the unit cell dimensions from PXRD after each exchange. Data were also obtained for the guest-free frameworks by exchanging DMF

https://dx.doi.org/10.1021/jacs.0c03853
J. Am. Chem. Soc. 2020, 142, 14903−14913

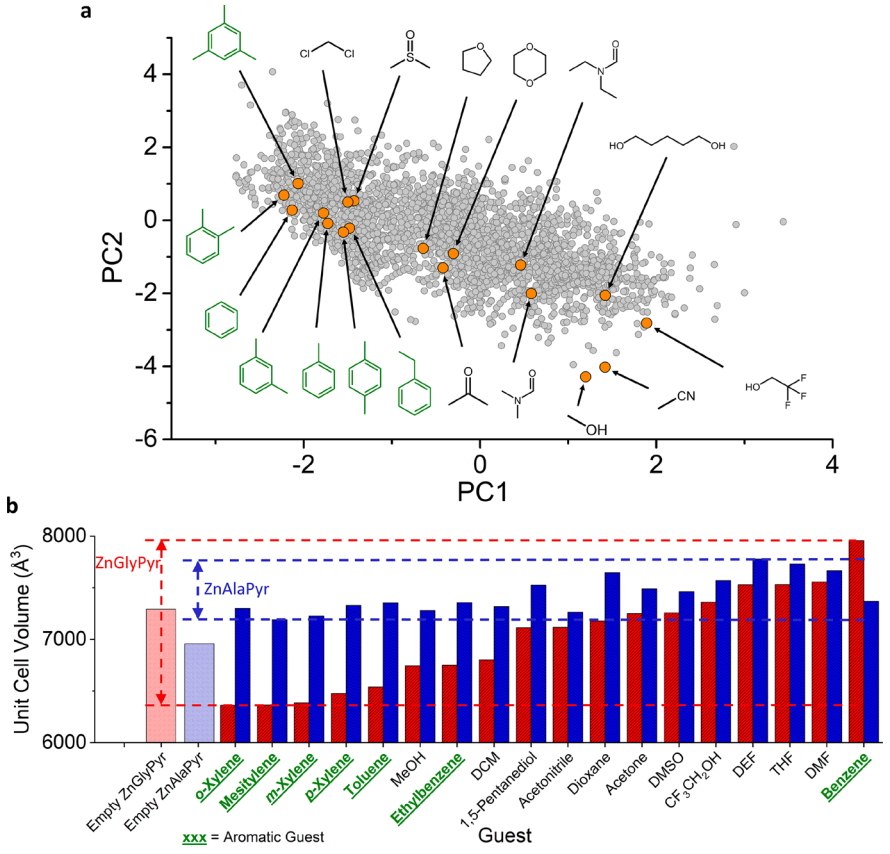

Figure 3. Structural response of ZnXPyr (X = Gly, Ala) to a library of guests. (a) The two-dimensional map of chemical space constructed using the principal components PC1 and PC2. The map guided the selection of molecules in the guest library used to investigate structural flexibility. (b) Comparison of the refined PXRD unit cell volumes of ZnGlyPyr (red) and ZnAlaPyr (blue) when they contain different liquid guests. The unit cell volume for both desolvated structures is also given (lightly shaded). The horizontal dashed lines in red and blue indicate the volume extrema observed for ZnGlyPyr and ZnAlaPyr, respectively.

with methanol and removing the guests by heating at 373 K under vacuum (see section S10 in the Supporting Information). To select the library of guests, 18 descriptors based on molecular size, shape, and intermolecular interactions were defined and calculated for 2982 known organic compounds with boiling points above 39 °C. Principal component analysis was then used to combine these descriptors into two generic orthogonal components (PC1 and PC2), providing a representation of the maximum separation of potential liquid guests in chemical space in two dimensions (Figure 3a). The selection of guests covers a broad range of this chemical space and allows the comparison of the structural response for each material with guests that have either very different (e.g., benzene vs MeOH) or very similar (e.g., benzene vs toluene) PC1 and PC2 values. These results are shown in Figure 3b (Tables S2 and S3), which displays the range of unit cell volumes obtained for all guests tested. ZnGlyPyr has a large volume range of 6363−7958 Å^3, while ZnAlaPyr shows a much narrower range of 7189−7778 Å^3. The guest-free structure of ZnGlyPyr lies between the volume extrema at 7285 Å^3, which suggests that guests can trigger either an expansion or a contraction of the structure on the basis of their interactions with the framework and their packing inside the pore. ZnAlaPyr, meanwhile, has a guest-free structure with a volume lower than all those of guest-loaded structures at 6950 Å^3.

The refinement of SCXRD data collected from the frameworks exposed to the different guests shows that the frameworks retain their connectivity and *R*3*c* or *R*3 symmetry in all cases (Tables S7 and S8). They respond to the guests by modifying both the volume and shape (Figures S40 and S41) of their pores through conformational change of the linker (Figure 4a), which determines the bend of the ribbons (Figure 4b,c) and the degree of distortion from a regular hexagon: ρ ranges from 116.9° to 137.4° (Figure S42). These changes modify the dimensions of the central channel (6.2 to 9.2 Å) and peripheral pocket (4.2 to 6.0 Å). The pore size changes are larger than those seen in highly flexible peptide MOFs (3 Å in ZnGlyPyr in comparison to 1.6 Å in ZnGGH, GGH = glycine−glycine-L-histidine)[31] but are driven by small adjustments in the torsion angles (ω(C−N amide bond), 178.6° to 193.3°; φ, 79.6° to 92.7°; ψ, −140.6° to −146.7°), whereas torsion angles in ZnGGH change by 150°. This arises from the *etb* topology, where the local changes in the conformation at each (GlyPyr)$^{2-}$ linker are globally amplified by the 6-fold geometry of the pore and the sensitivity of the pore volume and shape to even a small linker conformational change.

Aromatic guests produce the greatest unit cell volume range for ZnGlyPyr, with both unusually large (benzene) and unusually small (all other aromatics) volumes in comparison to other guests. The volumes observed for ZnAlaPyr with these aromatic guests lie in a much narrower range, which is also in line with the ZnAlaPyr structures observed for all other liquid guests and the absence of contraction below the guest-free volume, in contrast to ZnGlyPyr (Figure 3b). The volume change and guest uptake in ZnGlyPyr, and its contrast with ZnAlaPyr for a particular guest, do not however simply relate

https://dx.doi.org/10.1021/jacs.0c03853
J. Am. Chem. Soc. 2020, 142, 14903−14913

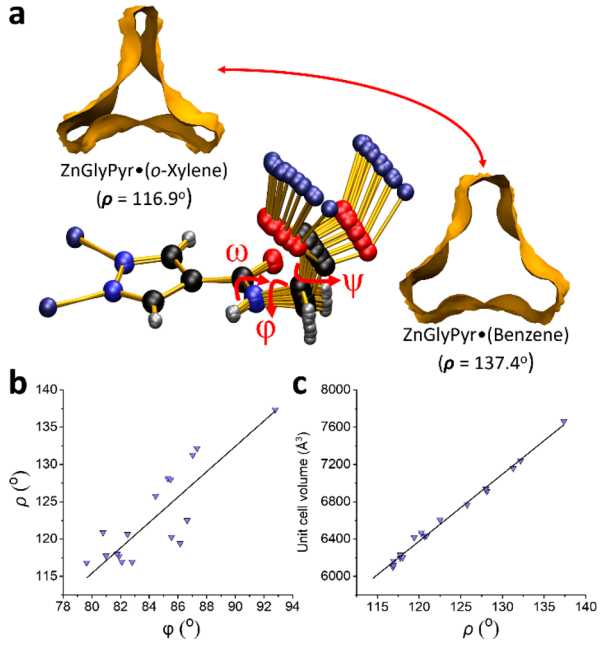

Figure 4. Variation of linker conformation in ZnGlyPyr with guests. (a) Overlay showing the changing conformation of the $(GlyPyr)^{2-}$ linkers in the ZnGlyPyr structures, based on SCXRD structures of ZnGlyPyr containing different liquid guests. This change in linker conformation produces an extensive transformation in pore size and shape from a contracted pore in ZnGlyPyr•(*o*-Xylene) to the most expanded form in ZnGlyPyr•(Benzene), as illustrated by the solvent-accessible voids. (b) Variation of bend of the H-bonded ribbons (ρ) with linker torsion φ for different liquid guests. (c) Variation of unit cell volume with ρ in these structures (Table S10).

to guest chemistry, because the feedback between guest uptake and host structure is determined by the host−guest system in each case. This can be understood by considering the refined SCXRD structures of both hosts with toluene and benzene.

Toluene in ZnGlyPyr•(Toluene) sits in a narrow peripheral pocket (Figure 5a) formed by a large bend (ρ = 118.0°) in the H-bonded ribbons produced by a torsional distortion of the linker that is greater than with nonaromatic guests. This results in pronounced shrinkage of the unit cell volume to 6539 Å^3 (PXRD) from 7285 Å^3 of the guest-free structure. The C$\alpha\cdots$C$_p$ (the carbon on the pyrazolate ring connecting to the amide group) distance at the pinch point becomes 3.7 Å, just wide enough to accommodate the toluene (Figure 5a inset and Figure S43). The plane of the aromatic ring is rotated 20° from parallel to the channel direction, forming $\pi-\pi$ interactions with the pyrazolate rings of the framework on one side and C−H to π interactions with the linker Cα on the other. The methyl groups in ZnAlaPyr, which are located at the pinch point, prevent ZnAlaPyr•(Toluene) from displaying the same response. The hypothetical structure of ZnAlaPyr•(Toluene) (Figure 5b), modeled at the same unit cell volume as for ZnGlyPyr•(Toluene), shows that the C$_{Me}\cdots$C$_p$ distance at the pinch point is 3.0 Å, which is insufficient for a toluene molecule. In order to accommodate the guests, the observed unit cell volume of ZnAlaPyr•(Toluene) (Figure 5c) is therefore significantly expanded to 7354 Å^3 by a change in ρ to 128.9° that widens the central channel and the pocket simultaneously. The C$_{Me}\cdots$C$_p$ distance at the pinch point becomes 4.1 Å and allows the toluene to rotate around the channel direction (c axis) by 60° in comparison to ZnGlyPyr•(Toluene), affording a T-shaped $\pi-\pi$ interaction with two adjacent pyrazolate rings (the toluene aromatic ring plane remains almost parallel to the channel direction, rotated by 11° from it, Figure S52). Vapor sorption shows that this expansion affords a larger toluene uptake by ZnAlaPyr (40.4 wt %) than by ZnGlyPyr (34.2 wt %) (Figure 5e). The methyl side chain, rather than reducing guest uptake through simple volume exclusion, is relocated to allow the guest to occupy its optimal position in the pocket. This requires a conformational change in the linker that, while it is driven by the local interaction with the guest, necessarily alters the global pore volume as both the pockets and the central channel expand.

ZnGlyPyr•(Benzene) (Figure 5d) shows the largest unit cell volume of all the structures studied (7958 Å^3, ρ = 137.4°), resulting from a very wide peripheral pocket where the C$\alpha\cdots$C$_p$ distance increases to 6.2 Å. This expanded pocket is accessed by the most extended linker conformation observed, which allows several different orientations of the benzene rings. Three different benzene environments are observed crystallographically (Figure 5d inset), including one where the plane of the aromatic ring is perpendicular to the channel direction (orange molecule in Figure 5d). In contrast to the lower volume aromatic structures discussed above, ZnGlyPyr organizes the benzene guests into a more extended unit through host−guest−guest interactions directly connected to the linker conformation. $\pi-\pi$ interactions between a pyrazolate ring on the walls of the framework and one of the benzene sites (green in Figure 5d) locate this first molecule within the peripheral pocket. T-shaped $\pi-\pi$ interactions with this site then localize the other two guest sites that extend toward the central channel (orange and cyan in Figure 5d). Such central channel species are disordered in the other refined structures, reflecting the more extensive dynamic possibilities in that less constrained part of the structure, and emphasize the specific extended intermolecular interactions that produce this commensurate packing[45,46] of the benzene guests in ZnGlyPyr. The extra methyl group in ZnAlaPyr would require a more significant expansion of the pore (predicted volume ∼8300 Å^3) to accommodate these benzene sites. This is disfavored because it would distort the metal−linker binding (see section S13 in the Supporting Information); thus, ZnAlaPyr adopts a lower volume structure with benzene (7370 Å^3, ρ = 130.2°) very similar to that found for toluene and exhibits lower (40.0 wt %) benzene uptake than ZnGlyPyr (54.3 wt %) (Figure 5f).

The adsorption of benzene vapors in ZnGlyPyr shows a two-step feature, indicating a phase transition process. *In situ* PXRD experiments were conducted to track the structural changes during this sorption process (see section S14 in the Supporting Information). The unit cell refinement against the PXRD patterns at different benzene loadings confirmed the structural transformations from the guest-free structure with unit cell volume 7241 Å^3 to a small-volume phase (6468 Å^3) at P/P_0 = 0.77 and then to a large-volume phase (7920 Å^3) at P/P_0 = 1. Rietveld refinement of the structure model at P/P_0 = 0.77 and *in situ* SCXRD desolvation experiments of ZnGlyPyr•(Benzene) (see section S10 in the Supporting Information) revealed that the partially loaded phase with benzene has the same structure feature as ZnGlyPyr•(Toluene), where the primary adsorption site lies in the same position as toluene in the pocket of the trefoil-shaped pore (Figure S57). This further confirms that ZnGlyPyr can adapt its pore shape and geometry when the guest loading is varied.

https://dx.doi.org/10.1021/jacs.0c03853
J. Am. Chem. Soc. 2020, 142, 14903−14913

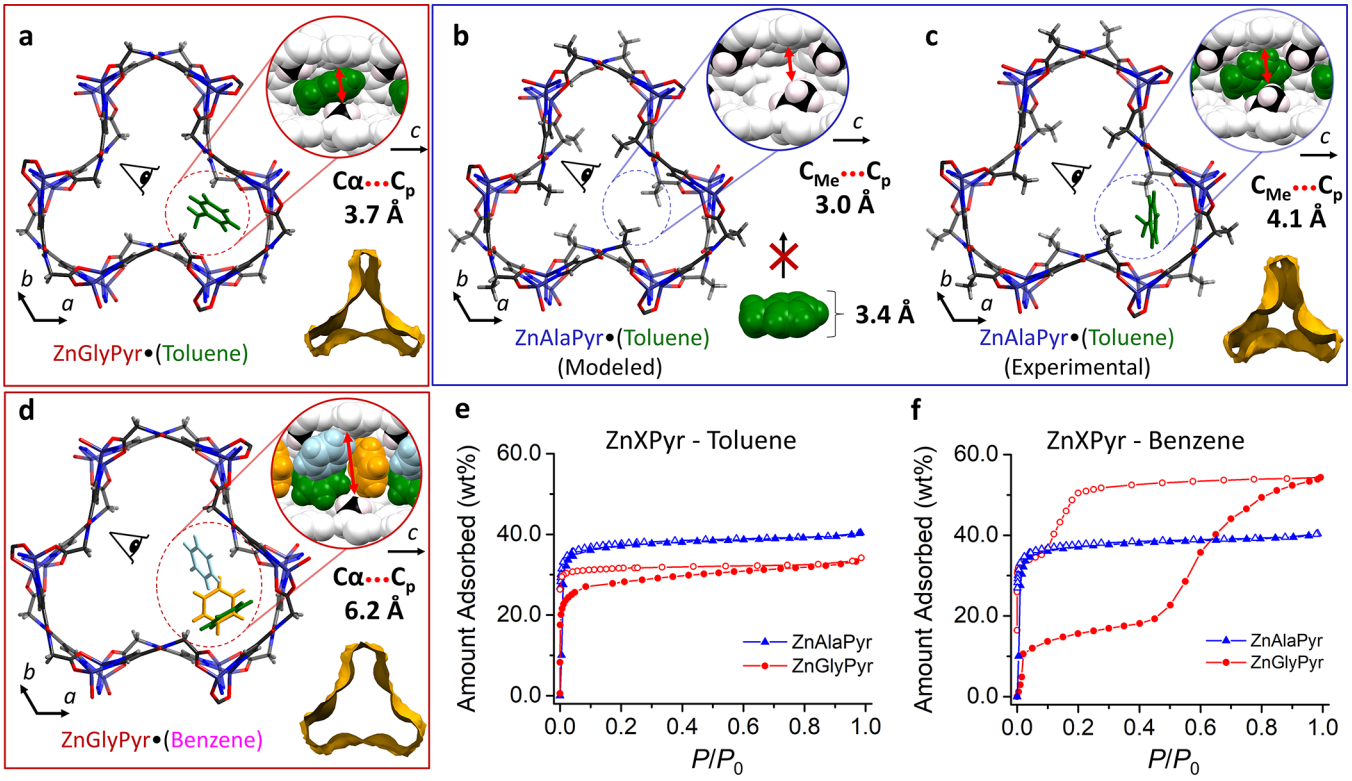

Figure 5. Linker conformation and side chain−guest interaction control structural response of ZnXPyr (X = Gly, Ala). (a) Refined SCXRD structure, guest packing in one peripheral pocket (inset), and solvent-accessible void (below and right) for ZnGlyPyr•(Toluene). Only the guest molecules in one pocket of the channel are shown for clarity. (b) DFT-minimized structure of ZnAlaPyr calculated at a fixed unit cell volume of 6200 Å^3. This is close to the unit cell volume of ZnGlyPyr•(Toluene) (6202 Å^3) and therefore provides an approximation to the structure of ZnAlaPyr•(Toluene) were it to adopt the same structure as its Gly analogue. The size of one toluene molecule is shown on the bottom right to demonstrate that this structure would be unable to fit a toluene molecule in the peripheral pocket because of the added side chain methyl group. (c) SCXRD structure, guest packing in one peripheral pocket (inset), and solvent-accessible surface (below and right) for the experimentally observed ZnAlaPyr•(Toluene) structure. (d) Single-crystal X-ray structure, guest packing in one peripheral pocket (inset), and solvent-accessible surface (bottom and right) for ZnGlyPyr•(Benzene). Atom colors: C, gray; H, light gray; N, blue; O, red; Zn, indigo. (e) Toluene vapor sorption isotherms for ZnGlyPyr (red) and ZnAlaPyr (blue) at 293 K. (f) Benzene vapor sorption isotherms for ZnGlyPyr (red) and ZnAlaPyr (blue) at 293 K.

The coupling of the trefoil-shaped pore with side chain chemistry in the ZnXPyr frameworks induces complex guest responses realized by modifying the torsional state of the linkers. The arrangement of guests in the peripheral pockets of the framework determines the accessible pore volume and total guest uptake by locally defining the optimal linker conformation. The interaction of guests with both the side chain and the rest of the pore surface chemistry gives extreme sensitivity of response to the host−guest system. Uptake of toluene by ZnAlaPyr is thus higher than by ZnGlyPyr because a guest interaction with the methyl side chain drives the overall pore expansion via changes in linker torsions. ZnAlaPyr, however, adsorbs considerably less benzene than ZnGlyPyr because the methyl side chain would require an unfavorable conformational change to accommodate the specific benzene packing seen for ZnGlyPyr. The distinct packing of benzene in ZnGlyPyr contrasts with that of all the other aromatics studied and reflects its specific match to a linker conformation that both optimizes local contact to the pore surface in the pocket and the extensive guest organization further into the central channel via the now-expanded pinch point. This is not observed for larger aromatics in ZnGlyPyr or for any guests in ZnAlaPyr, reflecting the decisive role of a host−guest chemical match within the pockets of the trefoil-shaped pores.

CO_2 Adsorption and *In Situ* PXRD Studies. Further differences in the behavior of ZnGlyPyr and ZnAlaPyr were observed upon the adsorption and desorption of CO_2 at 195 K. While both materials show similar saturated uptakes, 50.7 and 46.5 wt %, respectively, and display two-step adsorption isotherms (Figure 6a,b), the pressure of CO_2 at which the second step occurs is significantly different (40 mbar vs 200 mbar, respectively), and the final removal of CO_2 results in two completely different guest-free structures. This behavior was monitored *in situ* using PXRD (see section S16 in the Supporting Information): unit cell volumes indicating the structural changes are shown in Figure 6c,d and Tables S13 and S14. At low loadings of CO_2 (20−40 mbar, stage B in Figure 6c,d), ZnGlyPyr and ZnAlaPyr shrank to volumes of 5279.5 and 5106.5 Å^3, respectively, significantly smaller than those of the original desolvated materials (stage A, 7285/6950 Å^3) or any observed with liquid guests (6363−7958 Å^3). Both frameworks then expanded after exposure to CO_2 pressures above the gate pressure observed in each isotherm (stage C; 6119 Å^3 for ZnGlyPyr at 100 mbar and 6766 Å^3 for ZnAlaPyr at 300 mbar). During desorption, both materials showed a transition to small-volume structures (stage D: 5388.1 Å^3 for ZnGlyPyr at 25 mbar and 5106.8 Å^3 for ZnAlaPyr at 20 mbar), with a hysteresis in structure change similar to that in the adsorption−desorption isotherm. Exposing the samples to high

https://dx.doi.org/10.1021/jacs.0c03853
J. Am. Chem. Soc. 2020, 142, 14903−14913

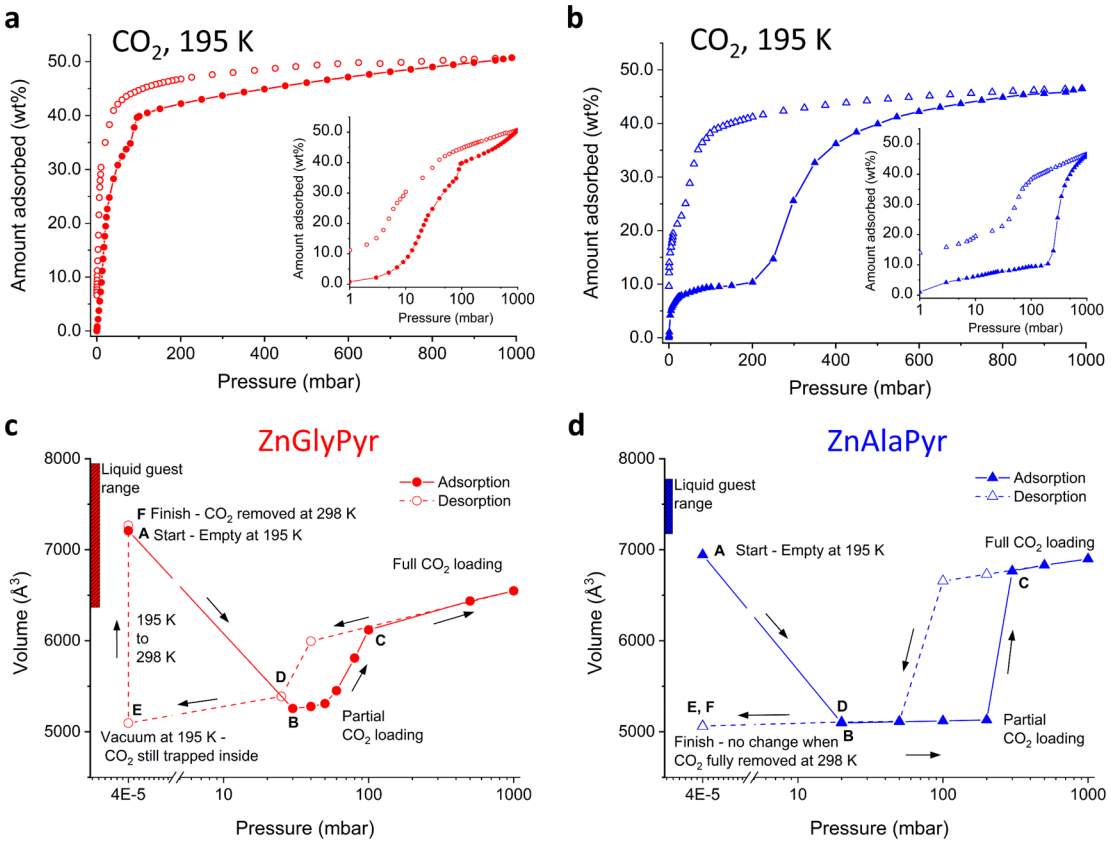

Figure 6. Sorption of CO_2 by ZnXPyr (X = Gly, Ala) leading to a new guest-free structure for X = Ala. (a) CO_2 adsorption−desorption isotherm for ZnGlyPyr (red spheres) at 195 K up to 1 bar. (b) CO_2 adsorption−desorption isotherm for ZnAlaPyr (blue triangles) at 195 K up to 1 bar. Solid markers denote adsorption and open markers desorption. Insets: isotherms plotted on a $\log_{10}$ scale. (c) Unit cell volumes of ZnGlyPyr (red spheres) obtained from Pawley refinements[47] based on *in situ* PXRD data as a function of CO_2 pressure. (d) Unit cell volumes of ZnAlaPyr (blue triangles) obtained from Pawley refinements based on *in situ* PXRD data as a function of CO_2 pressure. Solid markers denote adsorption and open markers desorption. Symbols A−F indicate the different stages of ZnXPyr during adsorption/desorption of CO_2.

vacuum, 10^{-5} mbar, at 195 K (stage E) was insufficient to remove all CO_2 from the pores; therefore at the end of each experiment the temperature was raised to 298 K (stage F) under high vacuum to complete CO_2 removal (Figures S59 and S60). At this point, the most significant divergence in the structural behavior of the two frameworks was observed. For ZnGlyPyr, the framework expands to the volume of the initial desolvated material (stage F, Figure 6c), while the removal of CO_2 from ZnAlaPyr leaves the framework highly contracted in a new guest-free phase (stage F, Figure 6d) of much smaller volume (5059 Å^3) in comparison to that accessed by desolvating structures containing liquid guests (6950 Å^3). This new small-volume ZnAlaPyr guest-free phase was not converted back to the original guest-free structure by heating at 450 K (Figure S62).

To understand this behavior, complete structural models for ZnGlyPyr and ZnAlaPyr at low CO_2 loadings were obtained by Rietveld refinement[48] (Figure 7a,b and Figures S63 and S67). CO_2 molecules were modeled with partial occupancies in both frameworks, equally distributed between the central channel and each peripheral pocket (Figures S64 and S70). Both compounds retained the same *etb* framework topology but had pore shapes highly distorted from a regular hexagon (ρ at 104.5° and 103.3°, respectively). These structures were accessed by the $(GlyPyr)^{2-}$ and $(AlaPyr)^{2-}$ linkers becoming more kinked by change in the ω torsion about the amide bond by 20° and 16°, respectively, in comparison to their starting desolvated structures. In contrast to the liquid guest-containing structures, the two components of the porosity are now isolated from each other, as there are boundaries between the central channel and the three pockets that the contained CO_2 guests cannot cross, shown by the solvent-accessible surfaces in Figure 7b. This segments the original single-pore geometry into four isolated components by a linker conformation change. Analysis of all MOF entries in the Cambridge Structural Database (see section S17 in the Supporting Information) suggests such a segmentation of the pore in response to changes in guests has not been previously observed. This segmentation of the pore demonstrates that the linker conformation is strongly coupled to the pore geometry (volume, shape, and connectivity) by the network structure and driven by the fit between the guests in the pocket and the shape of that pocket.

Refinement of the structure of the new small-volume, guest-free ZnAlaPyr phase showed that the segmented structure is retained, with further shrinkage of the pores in comparison to the CO_2-loaded material, resulting in the smallest central channel (2.5 Å) and narrowest peripheral pockets (1.2 Å) observed. There are short $C_{Me}\cdots C_{Me}$ contacts of 0.5 Å (with the vdW radii of the atoms taken into account) between the two closest Me groups at the pinch point, accessed via highly bent ribbons with a ρ value of 104.4°. This small-volume guest-free phase of ZnAlaPyr behaves very similarly to the original desolvated ZnAlaPyr in CO_2 sorption at 195 K, as shown by

https://dx.doi.org/10.1021/jacs.0c03853
J. Am. Chem. Soc. 2020, 142, 14903−14913

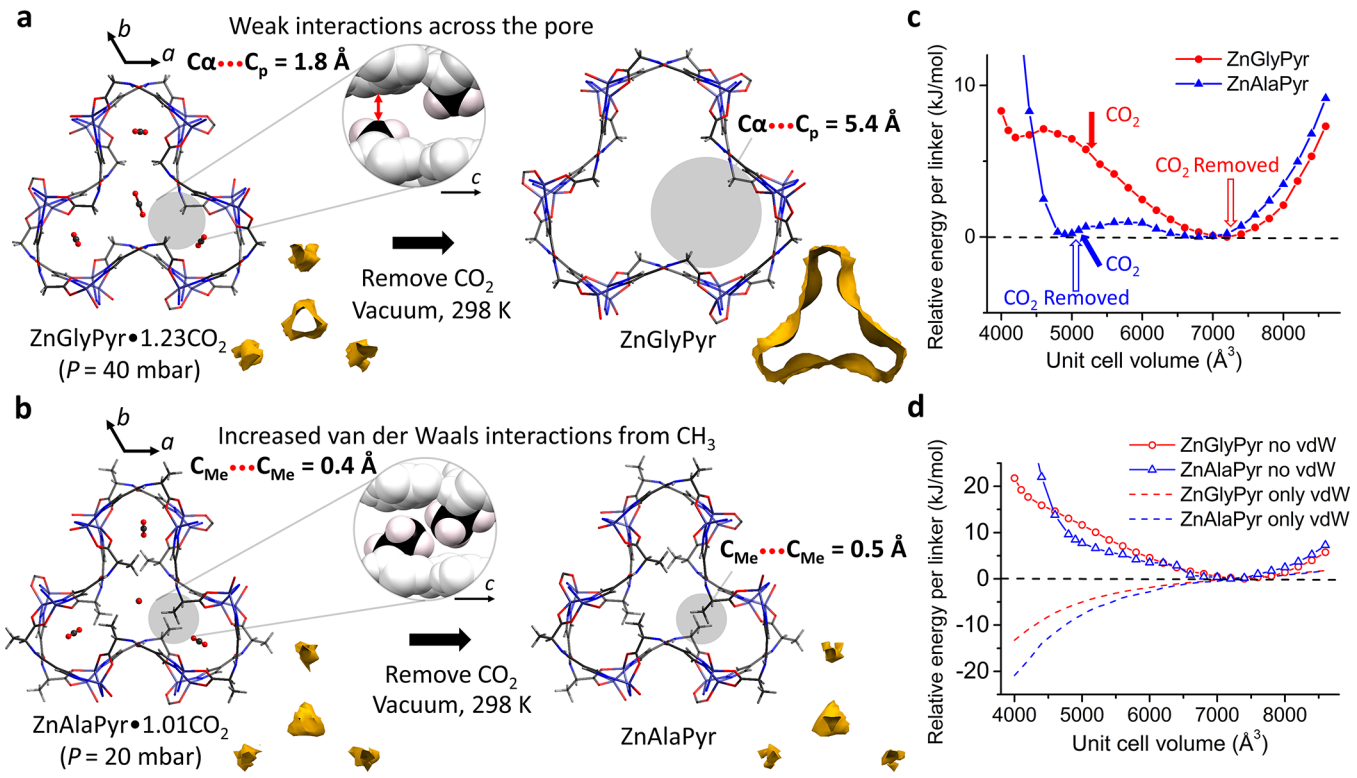

Figure 7. Response of ZnXPyr to removal of CO_2. Calculated $E-V$ curves and the structures of ZnXPyr (X = Gly, Ala) with and without CO_2. (a) The structures of ZnGlyPyr at a low pressure of CO_2 (P = 40 mbar, obtained from Rietveld refinements against *in situ* PXRD patterns) and after removal of CO_2. The composition given below the CO_2 structure is the refined value from the diffraction data at 40 mbar. For comparison, the composition at the same pressure obtained from gravimetric gas adsorption is ZnGlyPyr·1.49CO_2. The C···C distance is measured between the two closest C atoms across the pinch point. (b) The structures of ZnAlaPyr at a low pressure of CO_2 (P = 20 mbar) and after removal of CO_2, obtained from Rietveld refinements against *in situ* PXRD patterns. The composition given below the CO_2 structure is the refined value from the diffraction data at 20 mbar. For comparison, the composition at the same pressure obtained from gravimetric gas adsorption is ZnAlaPyr·1.19CO_2. The C···C distance is measured between the two closest methyl groups of the Ala moieties across the pinch point. In both (a) and (b) the solvent-accessible surfaces, calculated without guests, are shown below and to the right of each pore. The inset shows the interactions across one peripheral pocket in a space-filling representation. (c) Energy calculated using DFT for the relaxed framework structures of ZnGlyPyr (red circles) and ZnAlaPyr (blue triangles) sampled at differing unit cell volumes including vdW interactions. The arrows indicate the unit cell volumes observed experimentally at a low pressure of CO_2 and after full removal of CO_2 at 298 K from the two frameworks. (d) The two contributions to the total energy shown in (c) for ZnGlyPyr (red circles) and ZnAlaPyr (blue triangles)—interactions excluding vdW (solid lines) and the vdW components (dashed lines).

the isotherm collected using this new phase as the starting material (Figure S73). Interestingly, rapid removal of CO_2 from the material with a high CO_2 loading at 1000 mbar and 195 K resulted in a sample that contains both large- and small-volume structures (Figure S74). The small-volume phase was transformed to the previously described solvated phases ZnAlaPyr·MeOH and ZnAlaPyr•(Benzene) by immersing the sample in MeOH and benzene, respectively (Figure S75). After desolvation of both solvated samples at 100 °C for 1 h, the original large-volume guest-free structure was obtained.

Computational Analysis of Guest-Free ZnGlyPyr and ZnAlaPyr. The observed pore segmentation of both materials upon CO_2 sorption and the resulting new small-volume guest-free structure unique to ZnAlaPyr can be further understood with Density Functional Theory (DFT) calculations of the energy of the guest-free frameworks at different unit cell volumes (see section S18 in the Supporting Information). The resulting energy−unit cell volume ($E-V$) curves (Figure 7c) and the competition between the two constituent energy contributions, the elastic deformation of the framework, and the attractive vdW interactions (solid and dashed lines, respectively, in Figure 7d) reveal a clear difference between the two materials. ZnGlyPyr (red circles) has a global minimum at V = 7167 Å^3, corresponding well to the experimentally observed desolvated material (V = 7285 Å^3 at 298 K), and a second higher energy minimum at V = 4237 Å^3, suggesting a potential, but not experimentally observed, highly contracted guest-free material (closed form with no guests present). In contrast, ZnAlaPyr (blue triangles) shows two minima of almost equal energy at 6799 and 4961 Å^3. They correspond to the experimentally observed guest-free structures at 6950 Å^3 (after removal of MeOH at 298 K) and 5059 Å^3 (after removal of CO_2 at 298 K). Thus, different guest molecules permit navigation of the energy landscape of ZnAlaPyr to drive the material into one of the two structures that are stable upon guest removal.

The $E-V$ curves for the guest-free structures allow a rationalization of the differences between the ZnGlyPyr and ZnAlaPyr frameworks during removal of CO_2. In both materials, CO_2−host interactions overcome linker conformational energy penalties to afford cell volumes considerably smaller than those seen for liquid guests (Figure 3), forming a distinct set of structures where the peripheral pockets are isolated from the central channel to form a four-component pore topology as they encapsulate the CO_2 guests (Figure 7).

https://dx.doi.org/10.1021/jacs.0c03853
J. Am. Chem. Soc. 2020, 142, 14903−14913

When CO_2 is removed from the pores of the two materials, each framework follows the $E-V$ curve downhill toward the nearest local energy minimum (Figure 7c). Guest-free ZnGlyPyr cannot be stabilized with the linker in the highly kinked conformation due to the torsional strain and relaxes to the large volume minimum, corresponding to the single-component pore desolvated structure also formed by removal of the larger guests (Figure 7a). Conversely, ZnAlaPyr accesses the small-volume guest-free form with four isolated pore components (Figure 7b) very close in volume to the CO_2-containing start point because the Ala side chains produce stabilizing attractive Me···Me vdW interactions that overcome the higher linker torsional energy required to place them in these positions.

CONCLUSION

The ZnXPyr family of flexible MOFs derived from the amino acid residues X = Gly, Ala have an unusual trefoil-shaped porosity where a pinch point connects a central channel to three peripheral pockets. The pockets restructure through a linker conformational adjustment to both fit and be fitted by the guest packing: e.g., encapsulating CO_2 in a segmented porosity that arises from an extremely strained linker torsional state. This coupling of the local linker conformation, global pore geometry, and guest packing determines the ZnXPyr guest uptake and host structure response. The contrast in host volume change of and guest uptake by ZnGlyPyr between benzene and toluene shows how the host–guest chemistry precisely controls the response of the whole system.

The feedback among the pore structure, linker conformation, and guest packing also allows strong side chain control of the host response to the pore species. For example, the second guest-free structure observed only in ZnAlaPyr is stabilized by methyl–methyl interactions and ZnAlaPyr adsorbs more toluene than ZnGlyPyr, but less benzene. This side chain regulation of host–guest systems governed by single bond rotations has analogies in proteins, such as the contrast between the structure-forming role of Ala in α-helices and the diverse structural response associated with Gly. This indicates an opportunity to construct flexible frameworks that build in strong coupling of the guest and host from a synergy between the linker conformational change and pore reconfiguration to direct function. This can exploit side chain chemistries that span the diversity accessible to proteins to maximize control.

ASSOCIATED CONTENT

Supporting Information

The Supporting Information is available free of charge on the ACS Publications Web site. The Supporting Information is available free of charge at https://pubs.acs.org/doi/10.1021/jacs.0c03853.

Experimental procedures, single-crystal and powder X-ray diffraction experiments, gas and vapor adsorption measurements, detailed structural analyses and descriptions, computational details, and supporting figures and tables as detailed in the text (PDF)

CIF data for all of the structures (ZIP)

AUTHOR INFORMATION

Corresponding Author

Matthew J. Rosseinsky − *Department of Chemistry, University of Liverpool, Liverpool L69 7ZD, U.K.;* orcid.org/0000-0002-1910-2483; Email: rossein@liverpool.ac.uk

Authors

Yong Yan − *Department of Chemistry, University of Liverpool, Liverpool L69 7ZD, U.K.;* orcid.org/0000-0002-7926-3959

Elliot J. Carrington − *Department of Chemistry, University of Liverpool, Liverpool L69 7ZD, U.K.;* orcid.org/0000-0001-8855-809X

Rémi Pétuya − *Department of Chemistry, University of Liverpool, Liverpool L69 7ZD, U.K.;* orcid.org/0000-0002-3118-6966

George F. S. Whitehead − *Department of Chemistry, University of Liverpool, Liverpool L69 7ZD, U.K.;* orcid.org/0000-0003-1949-4250

Ajay Verma − *Department of Chemistry, University of Liverpool, Liverpool L69 7ZD, U.K.;* orcid.org/0000-0001-8085-7351

Rebecca K. Hylton − *Department of Chemistry, University of Liverpool, Liverpool L69 7ZD, U.K.*

Chiu C. Tang − *Diamond Light Source, Harwell Science and Innovation Campus, Didcot, Oxfordshire OX11 0DE, U.K.*

Neil G. Berry − *Department of Chemistry, University of Liverpool, Liverpool L69 7ZD, U.K.;* orcid.org/0000-0003-1928-0738

George R. Darling − *Department of Chemistry, University of Liverpool, Liverpool L69 7ZD, U.K.*

Matthew S. Dyer − *Department of Chemistry, University of Liverpool, Liverpool L69 7ZD, U.K.;* orcid.org/0000-0002-4923-3003

Dmytro Antypov − *Department of Chemistry, University of Liverpool, Liverpool L69 7ZD, U.K.;* orcid.org/0000-0003-1893-7785

Alexandros P. Katsoulidis − *Department of Chemistry, University of Liverpool, Liverpool L69 7ZD, U.K.;* orcid.org/0000-0003-0860-7440

Complete contact information is available at: https://pubs.acs.org/10.1021/jacs.0c03853

Notes

The authors declare no competing financial interest.

Crystallographic data for all of the structures have been deposited at the Cambridge Crystallographic Data Centre (CCDC), under the deposition numbers CCDC 1948777–1948822. Copies of these data can be obtained free of charge via www.ccdc.cam.ac.uk/data_request/cif. The data that support the findings of this study are available in the Research Data Catalogue of the University of Liverpool and can be found at http://datacat.liverpool.ac.uk/id/eprint/996.

ACKNOWLEDGMENTS

This project has received funding from the European Research Council (ERC) under the European Union's Horizon 2020 Research and Innovation Programme (grant agreement number 692685). We acknowledge the HEC Materials Chemistry Consortium funded by the EPSRC (EP/L000202, EP/R029431) for provision of computer time on the ARCHER UK National Supercomputing Service and on the

UK Materials and Molecular Modelling Hub, MMM Hub, which is partially funded by the EPSRC (EP/P020194). We thank the Diamond Light Source for provision of beam time on the I11 and I19 beamlines. D.A. thanks the Leverhulme Trust for funding via the Leverhulme Research Centre for Functional Materials Design. M.J.R. thanks the Royal Society for the award of a Research Professorship.

REFERENCES

(1) Warren, J. E.; Perkins, C. G.; Jelfs, K. E.; Boldrin, P.; Chater, P. A.; Miller, G. J.; Manning, T. D.; Briggs, M. E.; Stylianou, K. C.; Claridge, J. B.; Rosseinsky, M. J. Shape Selectivity by Guest-Driven Restructuring of a Porous Material. *Angew. Chem., Int. Ed.* **2014**, *53*, 4592−4596.

(2) Carrington, E. J.; McAnally, C. A.; Fletcher, A. J.; Thompson, S. P.; Warren, M.; Brammer, L. Solvent-Switchable Continuous-Breathing Behavior in a Diamondoid Metal−Organic Framework and Its Influence on CO_2 versus CH_4 Selectivity. *Nat. Chem.* **2017**, *9*, 882−889.

(3) Zhou, D.-D.; Chen, P.; Wang, C.; Wang, S.-S.; Du, Y.; Yan, H.; Ye, Z.-M.; He, C.-T.; Huang, R.-K.; Mo, Z.-W.; Huang, N.-Y.; Zhang, J.-P. Intermediate-Sized Molecular Sieving of Styrene from Larger and Smaller Analogues. *Nat. Mater.* **2019**, *18*, 994−998.

(4) Chang, Z.; Yang, D.-H.; Xu, J.; Hu, T.-L.; Bu, X.-H. Flexible Metal−Organic Frameworks: Recent Advances and Potential Applications. *Adv. Mater.* **2015**, *27*, 5432−5441.

(5) Chen, L.; Ye, J.-W.; Wang, H.-P.; Pan, M.; Yin, S.-Y.; Wei, Z.-W.; Zhang, L.-Y.; Wu, K.; Fan, Y.-N.; Su, C.-Y. Ultrafast Water Sensing and Thermal Imaging by a Metal−Organic Framework with Switchable Luminescence. *Nat. Commun.* **2017**, *8*, 15985.

(6) Mason, J. A.; Oktawiec, J.; Taylor, M. K.; Hudson, M. R.; Rodriguez, J.; Bachman, J. E.; Gonzalez, M. I.; Cervellino, A.; Guagliardi, A.; Brown, C. M.; Llewellyn, P. L.; Masciocchi, N.; Long, J. R. Methane Storage in Flexible Metal−Organic Frameworks with Intrinsic Thermal Management. *Nature* **2015**, *527*, 357−361.

(7) Yang, Q.-Y.; Lama, P.; Sen, S.; Lusi, M.; Chen, K.-J.; Gao, W.-Y.; Shivanna, M.; Pham, T.; Hosono, N.; Kusaka, S.; Perry IV, J. J.; Ma, S.; Space, B.; Barbour, L. J.; Kitagawa, S.; Zaworotko, M. J. Reversible Switching Between Highly Porous and Nonporous Phases of an Interpenetrated Diamondoid Coordination Network That Exhibits Gate-Opening at Methane Storage Pressures. *Angew. Chem., Int. Ed.* **2018**, *57*, 5684−5689.

(8) Schneemann, A.; Bon, V.; Schwedler, I.; Senkovska, I.; Kaskel, S.; Fischer, R. A. Flexible Metal−Organic Frameworks. *Chem. Soc. Rev.* **2014**, *43*, 6062−6096.

(9) Bezuidenhout, C. X.; Smith, V. J.; Esterhuysen, C.; Barbour, L. J. Solvent- and Pressure-Induced Phase Changes in Two 3D Copper Glutarate-Based Metal−Organic Frameworks via Glutarate (*+gauche* ⇄ *− gauche*) Conformational Isomerism. *J. Am. Chem. Soc.* **2017**, *139*, 5923−5929.

(10) Krause, S.; Bon, V.; Senkovska, I.; Stoeck, U.; Wallacher, D.; Többens, D. M.; Zander, S.; Pillai, R. S.; Maurin, G.; Coudert, F.-X.; Kaskel, S. A Pressure-Amplifying Framework Material with Negative Gas Adsorption Transitions. *Nature* **2016**, *532*, 348−352.

(11) Ortiz, A. U.; Boutin, A.; Gagnon, K. J.; Clearfield, A.; Coudert, F.-X. Remarkable Pressure Responses of Metal−Organic Frameworks: Proton Transfer and Linker Coiling in Zinc Alkyl Gates. *J. Am. Chem. Soc.* **2014**, *136*, 11540−11545.

(12) Sato, H.; Kosaka, W.; Matsuda, R.; Hori, A.; Hijikata, Y.; Belosludov, R. V.; Sakaki, S.; Takata, M.; Kitagawa, S. Self-Accelerating CO Sorption in a Soft Nanoporous Crystal. *Science* **2014**, *343*, 167−170.

(13) Zhang, Z.; Wojtas, L.; Eddaoudi, M.; Zaworotko, M. J. Stepwise Transformation of the Molecular Building Blocks in a Porphyrin-Encapsulating Metal−Organic Material. *J. Am. Chem. Soc.* **2013**, *135*, 5982−5985.

(14) Sarkisov, L.; Martin, R. L.; Haranczyk, M.; Smit, B. On the Flexibility of Metal−Organic Frameworks. *J. Am. Chem. Soc.* **2014**, *136*, 2228−2231.

(15) Zeng, Q.; Wang, K.; Zou, B. Large Negative Linear Compressibility in $InH(BDC)_2$ from Framework Hinging. *J. Am. Chem. Soc.* **2017**, *139*, 15648−15651.

(16) Yan, Y.; O'Connor, A. E.; Kanthasamy, G.; Atkinson, G.; Allan, D. R.; Blake, A. J.; Schröder, M. Unusual and Tunable Negative Linear Compressibility in the Metal−Organic Framework MFM-133(M) (M = Zr, Hf). *J. Am. Chem. Soc.* **2018**, *140*, 3952−3958.

(17) Serre, C.; Millange, F.; Thouvenot, C.; Noguès, M.; Marsolier, G.; Louër, D.; Férey, G. Very Large Breathing Effect in the First Nanoporous Chromium(III)-Based Solids: MIL-53 or $Cr^{III}(OH)\cdot\{O_2C-C_6H_4-CO_2\}\cdot\{HO_2C-C_6H_4-CO_2H\}_x\cdot H_2O_y$. *J. Am. Chem. Soc.* **2002**, *124*, 13519−13526.

(18) Maji, T. K.; Matsuda, R.; Kitagawa, S. A Flexible Interpenetrating Coordination Framework with a Bimodal Porous Functionality. *Nat. Mater.* **2007**, *6*, 142−148.

(19) Yang, S.; Lin, X.; Lewis, W.; Suyetin, M.; Bichoutskaia, E.; Parker, J. E.; Tang, C. C.; Allan, D. R.; Rizkallah, P. J.; Hubberstey, P.; Champness, N. R.; Thomas, K. M.; Blake, A. J.; Schröder, M. A Partially Interpenetrated Metal−Organic Framework for Selective Hysteretic Sorption of Carbon Dioxide. *Nat. Mater.* **2012**, *11*, 710−716.

(20) Zhang, J.-P.; Zhou, H.-L.; Zhou, D.-D.; Liao, P.-Q.; Chen, X.-M. Controlling Flexibility of Metal−Organic Frameworks. *Natl. Sci. Rev.* **2018**, *5*, 907−919.

(21) Frank, M.; Johnstone, M. D.; Clever, G. H. Interpenetrated Cage Structures. *Chem. - Eur. J.* **2016**, *22*, 14104−14125.

(22) Kubik, S. Anion Recognition in Aqueous Media by Cyclopeptides and Other Synthetic Receptors. *Acc. Chem. Res.* **2017**, *50*, 2870−2878.

(23) Eddaoudi, M.; Kim, J.; Rosi, N.; Vodak, D.; Wachter, J.; O'Keeffe, M.; Yaghi, O. M. Systematic Design of Pore Size and Functionality in Isoreticular MOFs and Their Application in Methane Storage. *Science* **2002**, *295*, 469−472.

(24) Ethiraj, J.; Albanese, E.; Civalleri, B.; Vitillo, J. G.; Bonino, F.; Chavan, S.; Shearer, G. C.; Lillerud, K. P.; Bordiga, S. Carbon Dioxide Adsorption in Amine-Functionalized Mixed-Ligand Metal−Organic Frameworks of UiO-66 Topology. *ChemSusChem* **2014**, *7*, 3382−3388.

(25) Ko, N.; Choi, P. G.; Hong, J.; Yeo, M.; Sung, S.; Cordova, K. E.; Park, H. J.; Yang, J. K.; Kim, J. Tailoring the Water Adsorption Properties of MIL-101 Metal−Organic Frameworks by Partial Functionalization. *J. Mater. Chem. A* **2015**, *3*, 2057−2064.

(26) Devic, T.; Horcajada, P.; Serre, C.; Salles, F.; Maurin, G.; Moulin, B.; Heurtaux, D.; Clet, G.; Vimont, A.; Grenèche, J.-M.; Le Ouay, B.; Moreau, F.; Magnier, E.; Filinchuk, Y.; Marrot, J.; Lavalley, J.-G.; Daturi, M.; Férey, G. Functionalization in Flexible Porous Solids: Effects on the Pore Opening and the Host-Guest Interactions. *J. Am. Chem. Soc.* **2010**, *132*, 1127−1136.

(27) Imaz, I.; Rubio-Martínez, M.; An, J.; Solé-Font, I.; Rosi, N. L.; Maspoch, D. Metal-Biomolecule Frameworks (MBioFs). *Chem. Commun.* **2011**, *47*, 7287−7302.

(28) Rabone, J.; Yue, Y.-F.; Chong, S. Y.; Stylianou, K. C.; Bacsa, J.; Bradshaw, D.; Darling, G. R.; Berry, N. G.; Khimyak, Y. Z.; Ganin, A. Y.; Wiper, P.; Claridge, J. B.; Rosseinsky, M. J. An Adaptable Peptide-Based Porous Material. *Science* **2010**, *329*, 1053−1057.

(29) Katsoulidis, A. P.; Park, K. S.; Antypov, D.; Martí-Gastaldo, C.; Miller, G. J.; Warren, J. E.; Robertson, C. M.; Blanc, F.; Darling, G. R.; Berry, N. G.; Purton, J. A.; Adams, D. J.; Rosseinsky, M. J. Guest-Adaptable and Water-Stable Peptide-Based Porous Materials by Imidazolate Side Chain Control. *Angew. Chem., Int. Ed.* **2014**, *53*, 193−198.

(30) Martí-Gastaldo, C.; Antypov, D.; Warren, J. E.; Briggs, M. E.; Chater, P. A.; Wiper, P. V.; Miller, G. J.; Khimyak, Y. Z.; Darling, G. R.; Berry, N. G.; Rosseinsky, M. J. Side-Chain Control of Porosity Closure in Single- and Multiple-Peptide-Based Porous Materials by Cooperative Folding. *Nat. Chem.* **2014**, *6*, 343−351.

https://dx.doi.org/10.1021/jacs.0c03853
J. Am. Chem. Soc. 2020, 142, 14903−14913

(31) Katsoulidis, A. P.; Antypov, D.; Whitehead, G. F. S.; Carrington, E. J.; Adams, D. J.; Berry, N. G.; Darling, G. R.; Dyer, M. S.; Rosseinsky, M. J. Chemical Control of Structure and Guest Uptake by a Conformationally Mobile Porous Material. *Nature* **2019**, *565*, 213−217.
(32) Yaghi, O. M.; Kalmutzki, M. J.; Diercks, C. S. Building Units of MOFs, In *Introduction to Reticular Chemistry: Metal−Organic Frameworks and Covalent Organic Frameworks*; Wiley-VCH: Weinheim, Germany, 2019.
(33) Pettinari, C.; Tăbăcaru, A.; Galli, S. Coordination Polymers and Metal−Organic Frameworks Based on Poly(pyrazole)-Containing Ligands. *Coord. Chem. Rev.* **2016**, *307*, 1−31.
(34) Masciocchi, N.; Galli, S.; Colombo, V.; Maspero, A.; Palmisano, G.; Seyyedi, B.; Lamberti, C.; Bordiga, S. Cubic Octanuclear Ni(II) Clusters in Highly Porous Polypyrazolyl-Based Materials. *J. Am. Chem. Soc.* **2010**, *132*, 7902−7904.
(35) Tonigold, M.; Lu, Y.; Mavrandonakis, A.; Puls, A.; Staudt, R.; Möllmer, J.; Sauer, J.; Volkmer, D. Pyrazolate-Based Cobalt(II)-Containing Metal−Organic Frameworks in Heterogeneous Catalytic Oxidation Reactions: Elucidating the Role of Entatic States for Biomimetic Oxidation Processes. *Chem. - Eur. J.* **2011**, *17*, 8671−8695.
(36) Blomberg, R.; Kries, H.; Pinkas, D. M.; Mittl, P. R. E.; Grütter, M. G.; Privett, H. K.; Mayo, S. L.; Hilvert, D. Precision is Essential for Efficient Catalysis in an Evolved Kemp Eliminase. *Nature* **2013**, *503*, 418−421.
(37) Ollikainen, N.; de Jong, R. M.; Kortemme, T. Coupling Protein Side-Chain and Backbone Flexibility Improves the Re-design of Protein-Ligand Specificity. *PLoS Comput. Biol.* **2015**, *11* (9), No. e1004335.
(38) Serrano, L.; Neira, J.-L.; Sancho, J.; Fersht, A. R. Effect of Alanine versus Glycine in α-Helices on Protein Stability. *Nature* **1992**, *356*, 453−455.
(39) Margarit, I.; Camagnoli, S.; Frigerio, F.; Grandi, G.; Filippis, D. V.; Fontana, A. Cumulative Stabilizing Effects of Glycine to Alanine Substitutions in Bacillus Subtilis Neutral Protease. *Protein Eng., Des. Sel.* **1992**, *5*, 543−550.
(40) Zou, J.; Song, B.; Simmerling, C.; Raleigh, D. Experimental and Computational Analysis of Protein Stabilization by Gly-to-D-Ala Substitution: A Convolution of Native State and Unfolded State Effects. *J. Am. Chem. Soc.* **2016**, *138*, 15682−15689.
(41) Scott, K. A.; Alonso, D. O. V.; Sato, S.; Fersht, A. R.; Daggett, V. Conformational Entropy of Alanine versus Glycine in Protein Denatured States. *Proc. Natl. Acad. Sci. U. S. A.* **2007**, *104*, 2661−2666.
(42) López-Llano, J.; Campos, L. A.; Sancho, J. α-Helix Stabilization by Alanine Relative to Glycine: Roles of Polar and Apolar Solvent Exposures and of Backbone Entropy. *Proteins: Struct., Funct., Genet.* **2006**, *64*, 769−778.
(43) Schoedel, A.; Li, M.; Li, D.; O'Keeffe, M.; Yaghi, O. M. Structures of Metal−Organic Frameworks with Rod Secondary Building Units. *Chem. Rev.* **2016**, *116*, 12466−12535.
(44) Liu, G. L.; Qin, Y. J.; Jing, L.; Wei, G. Y.; Li, H. Two Novel MOF-74 Analogs Exhibiting Unique Luminescent Selectivity. *Chem. Commun.* **2013**, *49*, 1699−1701.
(45) Smit, B.; Maesen, T. L. M. Commensurate "Freezing" of Alkanes in the Channels of a Zeolite. *Nature* **1995**, *374*, 42−44.
(46) Wu, H.; Gong, Q.; Olson, D. H.; Li, J. Commensurate Adsorption of Hydrocarbons and Alcohols in Microporous Metal Organic Frameworks. *Chem. Rev.* **2012**, *112*, 836−868.
(47) Pawley, G. S. Unit-Cell Refinement from Powder Diffraction Scans. *J. Appl. Crystallogr.* **1981**, *14*, 357−361.
(48) Rietveld, H. M. A Profile Refinement Method for Nuclear and Magnetic Structures. *J. Appl. Crystallogr.* **1969**, *2*, 65−71.

https://dx.doi.org/10.1021/jacs.0c03853
J. Am. Chem. Soc. 2020, 142, 14903−14913